Available online at www.sciencedirect.com
ScienceDirect
International Journal of Mechanical Sciences 49 (2007) 230–238
International Journal of MECHANICAL SCIENCES
www.elsevier.com/locate/ijmecsci

Heating of a uniform wafer disk

K.A. Seffen*, R.A. McMahon

Department of Engineering, University of Cambridge, Trumpington Street, Cambridge CB2 1PZ, UK

Received 31 July 2006; accepted 10 August 2006
Available online 26 September 2006

Abstract

The closed-form heating response of a thin uniform circular wafer is obtained, in view of a new processing method for semiconductor materials. A strain energy formulation is obtained expeditiously using Gaussian curvature and associated structural concepts. The method is developed for generally curved wafers, which accounts for flat, spherical, cylindrical and twisted shapes. Solutions for the first two types become available in closed form, and the deformation can exhibit a sudden change in axi-symmetrical response or a snap-through buckling, or both: for the latter two types, a numerical solution points to progressive deformation in both without buckling. All results are shown to compare rather well with finite element analysis.

Keywords: Heating; Semi-conductor wafer; Gaussian curvature; Buckling; Finite elements

1. Introduction

Recent innovations in the processing of semiconductor materials pose, rather fortuitously, some interesting and novel challenges in structural mechanics, which are addressed in this study. Of interest here is the rapid treatment of a film (≈ 35 nm) of cubic silicon carbide (SiC) on a thin disk (100 mm × 0.5 mm) of silicon by flashlamp irradiation [1] for ultimate use in high-integrity electrical devices. After being uniformly heated to 1000 °C, the composite silicon-SiC wafer suffers a pulse of high-energy radiation for about 20 ms: the intensity and shortness of pulse melts the silicon precisely beneath the film, enabling the dissipation of locked-in stresses, the removal of defects in the original SiC, and the subsequent epitaxial growth of superior SiC. Unfortunately, severe thermal gradients distort the wafer transversely, possibly seeding irrevocable shape changes and damage. However, the promise of drastically reduced processing times motivates an understanding of the limitations of manufacturing by this method, in pursuit of refinement and, ultimately lower production costs.

As a start, the non-linear thermal response for a given set of pulse attributes can be obtained by a diffusion equation approach [2] but deflexions do not feature, and accounting for them in a fully coupled, thermal elastic framework is not trivial. A simpler route assumes a de-coupled and quasi-statical performance, and is reasonable in view of the relative thinness of the wafer. The extremely thin SiC and melt layers do not disrupt the material homogeneity and isotropy within the wafer, which has the properties of silicon given in Table 1. Determining the wafer response under spatial variations of temperature is now sufficient, and here, they persist only in the direction z measured normal to the middle surface of the wafer, and are denoted by $T(z)$. In the absence of constraints, the wafer deflects initially into a uniform spherical "cap", of a curvature, κ, equal to [3].

$$\kappa_T = \int_{-t/2}^{t/2} z\alpha T(z)\,\mathrm{d}z \Big/ \int_{-t/2}^{t/2} z^2\,\mathrm{d}z, \tag{1}$$

where α is the linear coefficient of thermal expansion, and t is the total thickness. For moderately large deflexions under increasing κ_T, geometrical compatibility conditions demand the build-up of in-plane strains, and κ departs from Eq. (1) as the wafer begins to stiffen. Despite the simple geometry, a solution within an exact large-deflexion plate formulation [4] becomes intractable for constant

*Corresponding author. Tel.: +44 1223 764137; fax: +44 1223 332662.
E-mail address: kas14@cam.ac.uk (K.A. Seffen).

0020-7403/$ - see front matter © 2006 Elsevier Ltd. All rights reserved.
doi:10.1016/j.ijmecsci.2006.08.003

Nomenclature

a	water radius
D	flexural rigidity $= Et^3/12(1-\nu^2)$
E	Young's modulus
g	Gaussian curvature
M	bending moment
t	wafer thickness
T	temperature
U_B, U_S	stored strain energies in bending and stretching, respectively
$\bar{U}$	dimensionless strain energy $= U \times 12(1-\nu)a^2/E\pi t^5$
W	transverse displacement
x, y, z	materials coordinates
α	coefficient of thermal expansion
Δg	change in Gaussian curvature
ε_x, ε_y, γ_{xy}	middle surface strains
κ_x, κ_y, κ_{xy}	middle surface curvatures
χ_x, χ_y, χ_{xy}	change in curvatures
κ_T	integral heating parameter
$\bar{\kappa}$	dimensionless curvature $= \kappa \times a^2/t$
σ_x, σ_y, τ_{xy}	middle surface stresses
ϕ	dummy parameter $= (1-\nu)/16$
ν	Poisson's ratio

A superscript "*" denotes conditions at thermal buckling and a subscript "0" denotes initial quantities before heating.

thickness wafers, primarily, due to the development of a boundary layer near the free edge where the disappearing normal force and moment obviate a non-uniform deformation. Only *lenticular* wafers whose thickness tapers in a precise manner to zero on the edge [5] experience uniform deformation everywhere. Accordingly, the exact solution shows that, when the dimensionless spherical curvature reaches a value of $\sqrt{(14+2\nu)/(1+\nu)}$, where ν is the Poisson's ratio, the axi-symmetrical mode buckles suddenly into another mode with diverging principal curvatures, similar to the instant curling of a strip of paper placed on a domestic hot-plate.

These two regimes are confirmed experimentally by Mansfield using a pair of pre-stressed rubber disks of *constant* thicknesses, which are bonded together. Upon relaxing, they either curve uniformly or curl cylindrically, depending on the disparity of pre-stress between layers, and presumably, would exhibit a sudden switch between modes under progressive relaxation. This type of structural response is not surprising given that the interfacial mismatch between layers motivates the localised curving of material in the same way as heating does; see the Appendix for a formal confirmation. Furthermore, it suggests that boundary layer effects do not disrupt the prevalent deformation modes, as in the exact lenticular case, at least, if the disk is thin. A reasonable corollary to this assumption is that any non-uniform deformation near the edge may be neglected and, for modelling purposes, the agency of uniform curving, whether heating or locked-in stresses, can be assumed to induce uniform changes in curvature throughout, in order to simplify the analysis. For example, Freund [6] deals with pre-stressed wafer-film disks, similar to Mansfield's experiment, and captures their change in shape by a strain energy approach and not by solving complex partial differential equations of deformation. He finds a remarkably similar buckling curvature of $\sqrt{16/(1+\nu)}$ compared to Mansfield: the assumption of uniform curvature does, however, preclude the free-edge condition when deflexions are not small, and this may account for the difference in results.

Table 1
Properties of standard silicon wafer

Young's modulus, E	130 GPa
Poisson's ratio, ν	0.3
Thermal expansion coefficient, α	3.68×10^{-6} 1/K
Radius, a	50 mm
Thickness, t	0.5 mm

The aim of this paper is to present a compact description of the response of a uniform wafer (thin) disk under transverse thermal gradients, and to elucidate key features. The derivation uses a strain energy formulation and uniform changes in curvature for the bending performance, as per Freund [6], but the development thereafter is enhanced by strict concepts pertinent in the large-displacement behaviour of plates and shells, and not exploited by Freund. Attention is drawn, in particular, to the *Gaussian curvature* of the wafer, and its connection to the stretching behaviour using a well-known compatibility relationship; in so doing, the non-linear, strain–displacement relationships of von Karman [7] normally invoked for such problems need not be considered, which substantially curtails the analytical effort, as will be shown. The in-plane stretching stresses under curving are then extracted straightforwardly, for inclusion in the overall strain energy expression; but the process is framed in a general way, and therefore, can be extended without difficulty to a wafer with initial distortions, arising from deliberate or poor manufacturing conditions. The governing equations of deformation are obtained by variational means, giving way to a family of solutions enveloping Freund's case for a flat wafer and the snap-through buckling of a spherical wafer, first described by Wittrick et al. [8] in the behaviour of shallow bimetallic domes. Predictions for a range of wafer geometries, including singly curved (or cylindrical) and twisted wafers, are verified by finite element analysis, which does not make

the same simplifying assumptions of behaviour, and is a useful comparison. As a final remark, this work differs from that on Mansfield's lenticular disks in notable ways. The governing equations of deformation are derived from simpler energy considerations, which permit a closed-form description for uniform disks not reported previously. The bending-stretching interaction is quantified explicitly by the use of Gaussian curvature, which points immediately to solutions for the stretching behaviour *before* the governing equations are obtained, as the strain energy approach demands: this staggered approach helps to underpin the understanding of physical matters, and may usefully serve other studies of more complex *anisotropic* and possibly non-uniform disks, which exhibit similar large-deflexion instabilities during material activation, e.g. in the thermal curing of fibre-reinforced laminate plates [9].

2. Theoretical formulation and governing behaviour

For a point located in the middle surface of wafer at (x, y) from the centre, the initial distortion from the flat is $-w_0 = \kappa_{x0}x^2/2 + \kappa_{y0}y^2/2 + k_{xy0}xy$, and local gradients are small enough for κ_{x0} and κ_{y0} to be regarded as positive uniform curvatures in the x and y directions, respectively, and κ_{xy0} to be the associated twisting curvature. The corresponding Gaussian curvature [10] is $g_0 = \kappa_{x0}\kappa_{y0} - \kappa_{xy0}^2$. After deformation, the same point has displacement, $-w = \kappa_x x^2/2 + \kappa_y y^2/2 + \kappa_{xy}xy$, with Gaussian curvature, g equal to $\kappa_x\kappa y - \kappa_{xy}{}^2$. The uniform changes in curvature are therefore

$$\chi_x = \kappa_x - \kappa_{x0}, \quad \chi_y = \kappa_y - \kappa_{y0}, \quad \chi_{xy} = \kappa_{xy} - \kappa_{xy0} \tag{2}$$

and from Mansfield [3], the bending stress resultants per unit length in the same directions, accounting for κ_T from Eq. (1), are given as

$$\begin{aligned} M_x &= D[\chi_x + \upsilon\chi_y - (1+\nu)\kappa_T], \\ M_y &= D[\chi_y + \nu\chi_x - (1+\nu)\kappa_T], \\ M_{xy} &= D(1-\nu)\chi_{xy}, \end{aligned} \tag{3}$$

where D is the flexural rigidity equal to $Et^3/12(1-\nu^2)$ and E is the Young's modulus. It may be noted that Eq. (1) is assumed to be valid when the wafer is not initially flat, and when the bending stress resultants are zero everywhere, it may be verified that the changes in curvature, χ_x and χ_y, are equal to κ_T. Thus, for low levels of heating, the wafer can only deflect into a spherical mode with no external moment applied along the free edge by the support conditions, which are assumed to be simple henceforth.

As previously noted, the changes in curvature are expected to deviate from κ_T when the deflexions grow larger, and the bending moments in Eq. (3) are no longer zero, and wafer begins to store strain energy. An expression for the total strain energy is now sought by superposing separate, well-known components of bending and stretching energies in terms of middle-surface parameters whilst, for completeness, ensuring that the boundary conditions are proper and correct. Accounting for heating requires some modification of these components, but only in the bending sense, since heating is presumed to produce no in-plane distortions overall, for example, by having a linear temperature profile, from $+T$, say, to $-T$, at the two surfaces. The work done by the moments in Eq. (3) acting over the edges of an element can be integrated over the range of rotation, leading to the strain energy stored in bending per unit area, U_B, as

$$\begin{aligned} U_B = \frac{D}{2}[&(\chi_x + \chi_y)^2 - 2(1-\nu)(\chi_x\chi_y - \chi_{xy}^2) \\ &- 2(1+\nu)\kappa_T(\chi_x + \chi_y - \kappa_T)], \end{aligned} \tag{4}$$

which reduces to a familiar form [10] when terms in κ_T are omitted. Without applying an edge moment, then strictly speaking, U_B is not completely correct; but it may be argued that the width of the boundary layer is small enough in practice to be neglected, as it tends to be for thin plates and shells, and U_B is sufficiently accurate for present purposes: the matter needs a proper investigation outside of this study. The situation for membrane behaviour, however, is more rigorously addressed.

First, the positive in-plane stretching strains, ε_x and ε_y, and shear strain, γ_{xy}, for the middle surface must be compatible with its change in Gaussian curvature, $g-g_0$ denoted by Δg, in the following manner [10]

$$-\Delta g = \frac{\partial^2\varepsilon_x}{\partial y^2} + \frac{\partial^2\varepsilon_y}{\partial x^2} - \frac{\partial^2\gamma_{xy}}{\partial x\partial y}. \tag{5}$$

The resulting elastic laws for middle-surface stretching without in-plane heating effects are the familiar forms

$$\varepsilon_x = \frac{\sigma_x}{E} - \nu\frac{\sigma_y}{E}, \quad \varepsilon_y = \frac{\sigma_y}{E} - \nu\frac{\sigma_x}{E}, \quad \gamma_{xy} = \frac{2\tau_{xy}(1+\nu)}{E}, \tag{6}$$

where the corresponding normal stresses, σ_x and σ_y, and shear stress, τ_{xy}, can be written in terms of an Airy stress-function, Φ, such that [3]

$$\sigma_x = \frac{\partial^2\Phi}{\partial y^2}, \quad \sigma_y = \frac{\partial^2\Phi}{\partial x^2}, \quad \tau_{xy} = -\frac{\partial^2\Phi}{\partial x\partial y}. \tag{7}$$

Combining Eqs. (5)–(7) therefore presents an alternative statement of the bending–stretching interaction

$$-E\Delta g = \frac{\partial^4\Phi}{\partial x^4} + 2\frac{\partial^4\Phi}{\partial x^2\partial y^2} + \frac{\partial^4\Phi}{\partial y^4} \tag{8}$$

and since Δg does not depend on x and y, Φ can be taken as a general fourth order polynomial, giving way to quadratic stresses via Eq. (7). It may be verified that if Φ is selected as

$$\Phi = \frac{E\Delta g}{32}(x^2 + y^2)\left[a^2 - \frac{x^2 + y^2}{2}\right],$$

where a is the radius of wafer, Eq. (8) is satisfied, with

$$\sigma_x = -\frac{E\Delta g}{16}[x^2 + 3y^2 - a^2],$$
$$\sigma_y = -\frac{E\Delta g}{16}[y^2 + 3x^2 - a^2],$$
$$\tau_{xy} = \frac{E\Delta g}{16}\,2xy. \tag{9}$$

These expressions constitute an exact equilibrium solution in which the middle-surface stress components vanish on the free edge and the resultant force and shear force across any diameter—if the wafer were divided in half—is zero. Linear terms violate the necessary symmetry of solution and do not appear. These stresses can now be substituted into the familiar form of stretching stain energy density, U_S [10]

$$U_S = \frac{t}{2E}[(\sigma_x + \sigma_y)^2 - 2(1+\nu)(\sigma_x\sigma_y - \tau_{xy}^2)], \tag{10}$$

which is added to U_B, and integrated over the surface area of wafer, to reveal the total stored energy U. Defining dimensionless $\bar{U} = U \times 12(1-\nu)a^2/E\pi t^5$ and $\bar{\kappa} = \kappa \times a^2/t$, it can be shown that

$$\begin{aligned}\bar{U} = \frac{1}{2(1+\nu)}\{&(\bar{\kappa}_x + \bar{\kappa}_y - \bar{\kappa}_{x0} - \bar{\kappa}_{y0})^2 \\ &- 2(1-\nu)[(\bar{\kappa}_x - \bar{\kappa}_{x0})(\bar{\kappa}_y - \bar{\kappa}_{y0}) - (\bar{\kappa}_{xy} - \bar{\kappa}_{xy0})^2] \\ &- 2(1+\nu)\bar{\kappa}_T(\bar{\kappa}_x + \bar{\kappa}_y - \bar{\kappa}_{x0} - \bar{\kappa}_{y0} - \bar{\kappa}_T)\} \\ &+ \frac{1-\nu}{32}[\bar{\kappa}_x\bar{\kappa}_y - \bar{\kappa}_{x0}\bar{\kappa}_{y0} - \bar{\kappa}_{xy}^2 + \bar{\kappa}_{xy0}^2]^2.\end{aligned} \tag{11}$$

Statical equilibrium states of the wafer are furnished by stationary values of the energy $\partial\bar{U}/\partial\bar{\kappa}_x = 0$, $\partial\bar{U}/\partial\bar{\kappa}_y = 0$, and $\partial\bar{U}/\partial\bar{\kappa}_{xy} = 0$, and yield, respectively, after re-arrangement

$$\bar{\kappa}_x - \bar{\kappa}_{x0} + \nu(\bar{\kappa}_y - \bar{\kappa}_{y0}) + \bar{\kappa}_y(1+\nu)\phi\Delta\bar{g} = (1+\nu)\bar{\kappa}_T, \tag{12a}$$

$$\bar{\kappa}_y - \bar{\kappa}_{y0} + \nu(\bar{\kappa}_x - \bar{\kappa}_{x0}) + \bar{\kappa}_x(1+\nu)\phi\Delta\bar{g} = (1+\nu)\bar{\kappa}_T, \tag{12b}$$

$$(1-\nu)(\bar{\kappa}_{xy} - \bar{\kappa}_{xy0}) - \bar{\kappa}_{xy}(1+\nu)\phi\Delta\bar{g} = 0. \tag{12c}$$

Here, ϕ is equal to $(1-\nu)/16$. For prescribed κ_T, ν, κ_{x0}, κ_{y0} and κ_{xy0}, Eqs. (12a)–(12c) uniquely determine κ_x, κ_y and κ_{xy}. Despite the non-linearity wrought by $\Delta\bar{g}$ $(= \bar{\kappa}_x\bar{\kappa}_y - \bar{\kappa}_{x0}\bar{\kappa}_{y0} - \bar{\kappa}_{xy}^2 + \bar{\kappa}_{xy0}^2)$, it may be eliminated between Eqs. (12a) and (12b) to present the invariant, homogenous relationship between $\bar{\kappa}_x$ and $\bar{\kappa}_y$

$$\begin{aligned}&\bar{\kappa}_x^2 - \bar{\kappa}_y^2 - \bar{\kappa}_x(\bar{\kappa}_{x0} + \nu\bar{\kappa}_{y0}) + \bar{\kappa}_y(\nu\bar{\kappa}_{x0} + \bar{\kappa}_{y0}) \\ &\quad - (\bar{\kappa}_x - \bar{\kappa}_y)(1+\nu)\bar{\kappa}_T = 0.\end{aligned} \tag{13}$$

If $\bar{\kappa}_{x0} = \bar{\kappa}_{y0}$, equal to $\bar{\kappa}_0$, say, Eq. (13) has two linear factors and hence, two distinct modes of deformation

$$\bar{\kappa}_x - \bar{\kappa}_y = 0, \quad \bar{\kappa}_x + \bar{\kappa}_y - [1+\nu](\bar{\kappa}_0 + \bar{\kappa}_T) = 0. \tag{14}$$

The deformation for each case must also obey Eq. 12(c), whose character immediately becomes clear if attention is restricted to wafers with no initial twist; then there is either no resultant twist or the change in Gaussian curvature is constant:

$$\bar{\kappa}_{xy}[1 - \nu - (1+\nu)\phi\Delta\bar{g}] = 0 \Rightarrow \bar{\kappa}_{xy} = 0, \tag{15a}$$

or

$$\Delta\bar{g} = \frac{1-\nu}{\phi(1+\nu)}. \tag{15b}$$

Since the membrane stresses in Eq. (9) linearly depend upon $\Delta\bar{g}$, and the result in Eq. (15b) does not depend upon the level of heating, then it conforms to a *developable* deformation in which there is no further stretching or increase in the stretching strain energy. However, if the initial distortions are not axi-symmetrical, Eq. (13) does not factorise, and there is only one mode, of non-developable displacements.

In the following section, solutions are determined for a number of cases in which $\bar{\kappa}_{xy0}$ is chosen to be zero; whilst enabling the specific solutions of Eq. (15) for transparency, this feature does not preclude cases with initial twist if $\bar{\kappa}_{x0}$ and $\bar{\kappa}_{y0}$ are set equal but opposite, and is the last case. The first case is for a flat wafer and it reproduces Freund's result but confirms formally the developable post-buckling mode. The second considers a spherical wafer, which points to an interesting snap-through buckling. The third and fourth cases consider wafers initially cylindrical and saddle-shaped (twisted), and are numerical solutions without any bifurcation behaviour. In all cases, the results focus on the dimensionless edge displacements, d/t, at the ends of the x- and y-axes, which are principal displacements in the absence of twist and equal to $(\bar{\kappa}_x - \bar{\kappa}_{x0})/2$ and $(\bar{\kappa}_y - \bar{\kappa}_{y0})/2$, respectively, with $\bar{\kappa}_x > \bar{\kappa}_y$ unless stated otherwise.

3. Solutions

3.1. Flat wafer: Freund's case

When $\bar{\kappa}_{x0} = \bar{\kappa}_{y0} = 0$, Eq. (13) has the two solutions

$$\bar{\kappa}_x = \bar{\kappa}_y, \quad \bar{\kappa}_x + \bar{\kappa}_y = (1+\nu)\bar{\kappa}_T,$$

which are now considered separately.

For the first case, define $\bar{\kappa}_x = \bar{\kappa}_y = \bar{\kappa}$, and substitute back into either of Eqs. (12a) or (12b), whereupon $\bar{\kappa} + \bar{\kappa}\phi\Delta\bar{g} = \bar{\kappa}_T$. From Eq. (15), the change in Gaussian curvature is either $\bar{\kappa}^2$ for no twisting curvature or equal to a constant, $(1-\nu)/(1+\nu)\phi$, respectively, giving

$$\bar{\kappa} + \phi\bar{\kappa}^3 = \bar{\kappa}_T, \tag{16a}$$

$$\bar{\kappa} = \frac{(1+\nu)\bar{\kappa}_T}{2}. \tag{16b}$$

For the second case, choosing $\bar{\kappa}_{xy} = 0$ from Eq. (15) sets $\Delta\bar{g} = \bar{\kappa}_x\bar{\kappa}_y$ and, if substituted back into Eq. (12a) or (12b),

results in

(a) $\bar{\kappa}_y[1-\nu-(1+\nu)\phi\bar{\kappa}_x\bar{\kappa}_y]=0 \Rightarrow \bar{\kappa}_y=0,$

or

(b) $\bar{\kappa}_x\bar{\kappa}_y=\dfrac{1-\nu}{\phi(1+\nu)}.$

Solution (a) is an asymptote, clarified later, but (b) is the *same* solution as Eq. (15b); there is no twisting and no change in Gaussian curvature for this mode. The ultimate solutions can be verified as

$$\bar{\kappa}_x=\frac{(1+\nu)\bar{\kappa}_T}{2}\left(1+\left[1-\frac{64}{(1+\nu)^3\bar{\kappa}_T^2}\right]^{0.5}\right), \tag{17a}$$

$$\bar{\kappa}_y=\frac{(1+\nu)\bar{\kappa}_T}{2}\left(1-\left[1-\frac{64}{(1+\nu)^3\bar{\kappa}_T^2}\right]^{0.5}\right). \tag{17b}$$

Real values exist only if

$$\bar{\kappa}_T\geqslant\frac{8}{(1+\nu)^{3/2}}=\bar{\kappa}_T^* \quad \text{(say)}, \tag{18}$$

which offers the slightly more compact expressions

$$\bar{\kappa}_x=\frac{(1+\nu)\bar{\kappa}_T}{2}(1+[1-(\bar{\kappa}_T^*/\bar{\kappa}_T)^2]^{0.5}),$$
$$\bar{\kappa}_y=\frac{(1+\nu)\bar{\kappa}_T}{2}(1-[1-(\bar{\kappa}_T^*/\bar{\kappa}_T)^2]^{0.5}). \tag{19}$$

When $\bar{\kappa}_T=\bar{\kappa}_T^*$, both curvatures are equal to $(1+\nu)\bar{\kappa}_T^*/2$, as per Eq. 16(b), which ties the two cases together at a single value of heating. Examination of the strain energy confirms that less energy is stored during the axi-symmetrical mode for $\bar{\kappa}_T<\bar{\kappa}_T^*$ compared to the second mode, and vice versa; since the curvatures grow apart immediately after this point, the wafer shape undergoes a bifurcation, evident in the plotting of displacements later. The corresponding curvature is denoted as $\bar{\kappa}^*$, equal to $(1+\nu)\bar{\kappa}_T^*/2=4/\sqrt{1+\nu}$, and is identical to that found by Freund [6]. Thus, rotationally symmetrical deflexions and wafer stretching suddenly give way to inextensional behaviour and constant Gaussian curvature with respect to the conditions at bifurcation.

The "choice" of mode for a given heating level is formally dictated by its stability, which can be assessed by interrogating the generalised stiffness matrix, outlined in Guest and Pellegrino [11] for two solution variables. For three independent solution curvatures here, this matrix can be augmented without difficulty to yield the form

$$\begin{bmatrix} \partial^2\bar{U}/\partial\bar{\kappa}_x^2 & \partial^2\bar{U}/\partial\bar{\kappa}_x\partial\bar{\kappa}_y & \partial^2\bar{U}/\partial\bar{\kappa}_x\bar{\kappa}_{xy} \\ \partial^2\bar{U}/\partial\bar{\kappa}_y\partial\bar{\kappa}_x & \partial^2\bar{U}/\partial\bar{\kappa}_y^2 & \partial^2\bar{U}/\partial\bar{\kappa}_y\partial\bar{\kappa}_{xy} \\ \partial^2\bar{U}/\partial\bar{\kappa}_{xy}\partial\bar{\kappa}_x & \partial^2\bar{U}/\partial\bar{\kappa}_{xy}\partial\bar{\kappa}_y & \partial^2\bar{U}/\partial\bar{\kappa}_{xy}^2 \end{bmatrix}, \tag{20}$$

where each element corresponds to a generalised stiffness, following the required differentiation of Eq. (11). A particular mode of deformation is stable only when this matrix is positive definite, which can be assured, in turn, by *all* of its eigenvalues being positive. For example, it can be verified that the present case of spherical deformation without twist is stable provided

$$1+3\phi\bar{\kappa}^2>0, \quad \left(\frac{1-\nu}{1+\nu}\right)-\phi\bar{\kappa}^2>0$$

from the closed-form eigenvalues, otherwise when $\bar{\kappa}>4/\sqrt{1+\nu}=\bar{\kappa}^*$, the mode becomes unstable, leading to bifurcation. The stability of other modes in the rest of this paper are similarly confirmed but, for the sake of the brevity, their calculation is not performed explicitly suffice to assert the particular outcome.

Predictions are compared to a finite element analysis in Fig. 1 using the commercially available software package, ABAQUS [12]. In this solution, the wafer can deform elastically with non-uniform curvature, the bending moment is set to be zero along the free edge, and geometrical non-linearity is taken into account. A full mesh is constructed from a mixture of triangular and rectangular shell elements of bi-directional quadratic displacement fields and five spatial degrees-of-freedom per node. The nodal displacements are measured relative to the fixed central node, and heating is simulated by prescribing the linear temperature profile at all nodes, and increasing it from zero. The non-linear response is carefully determined from small strains using a dedicated Riks'algorithm [13], which searches for the correct equilibrium path using an arc-length method. The initial mesh is elliptically perturbed to introduce some geometrical asymmetry so that the finite

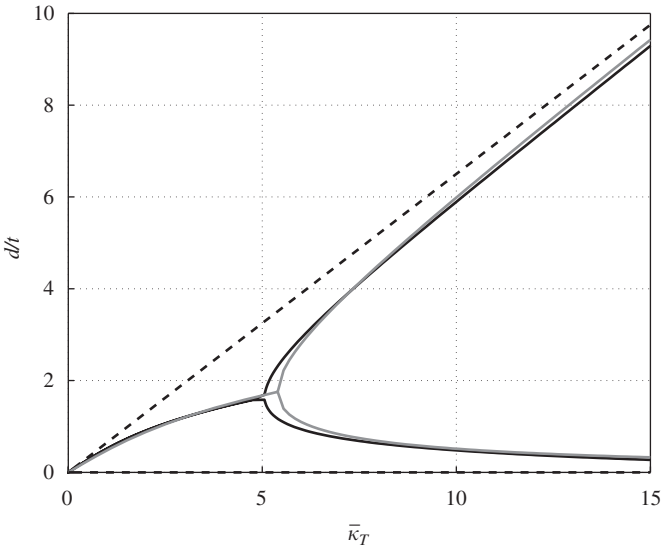

Fig. 1. Predictions of maximum and minimum out-of-plane displacements compared to finite element analysis of the standard wafer, Table 1. The grey line first details the solution of Eq. (16a) for pre-buckling, followed by Eqs. (17a) and (17b) for the post-buckled behaviour. The black solid lines are reproduced exactly from a finite element analysis for the indicated geometry of wafer but are difficult to see, due to the overlapping theoretical lines, except near to the bifurcation, around $\bar{\kappa}_T=5$. The dashed lines are approximate large displacement solutions found by setting $\bar{\kappa}_T^*=0$ in Eq. (19).

element solver may detect the post-buckled path; the major and minor axes lengths differ only by 0.1%, and is sufficiently small for the pre-buckling results to be indistinguishable from a perfectly circular wafer [14].

The correlation is very close throughout although there is some discrepancy in the bifurcation region; the theoretical value of $\bar{\kappa}_T^*$ is 5.39 for $\nu = 0.3$, compared to the finite element result of 5.05, and may be due to improper modelling of the free-edge conditions. General agreement is quickly restored at $\bar{\kappa}_T \approx 6$. For very large displacements, the asymptotic solutions to Eq. (19), $\bar{\kappa}_x = (1+\nu)\bar{\kappa}_T$ and $\bar{\kappa}_y = 0$, which conform to a purely cylindrical deformation, are reasonably good. If the direction of thermal gradients is reversed, the same behaviour is exhibited but with opposite-sense displacements.

3.2. Spherical wafer: Wittrick's case

For initially spherical wafers, $\bar{\kappa}_{x0} = \bar{\kappa}_{y0} = \bar{\kappa}_0$, Eq. (14) shows

$$\bar{\kappa}_x = \bar{\kappa}_y, \quad \bar{\kappa}_x + \bar{\kappa}_y = (1+\nu)[\bar{\kappa}_0 + \bar{\kappa}_T]$$

and are identical to the flat-wafer case if $\bar{\kappa}_0$ is set to zero, leading to the same responsive modes. In particular, the axi-symmetrical deformation has $\bar{\kappa}_x = \bar{\kappa}_y = \bar{\kappa}$ with $\Delta\bar{g} = \bar{\kappa}^2 - \bar{\kappa}_0^2$, and is governed by

$$\bar{\kappa}[1 - \phi\bar{\kappa}_0^2] + \phi\bar{\kappa}^3 - \bar{\kappa}_0 = \bar{\kappa}_T. \tag{21}$$

Interestingly, there are two stationary points and hence, two zero-stiffness configurations are provided if $\bar{\kappa}_0 > 1/\sqrt{\phi}$. In between these points, the equilibrium path has negative stiffness and is unstable under progressive heating, or cooling, as will be shown. *Without* heating, i.e. when $\bar{\kappa}_T = 0$, Eq. (21) may be factorised into

$$\phi\bar{\kappa}(\bar{\kappa}^2 - \bar{\kappa}_0^2) + \bar{\kappa} - \bar{\kappa}_0 = 0 \Rightarrow (\bar{\kappa} - \bar{\kappa}_0)[\phi\bar{\kappa}^2 + \phi\bar{\kappa}\bar{\kappa}_0 + 1] = 0,$$

with the following three roots

$$\bar{\kappa}_0, \quad -\frac{\bar{\kappa}_0}{2}\left[1 \pm \left(1 - \frac{4}{\phi\bar{\kappa}_0^2}\right)^{0.5}\right].$$

The first of these is the initial shape, and the other two are real *inverted* configurations if $\bar{\kappa}_0 > 2/\sqrt{\phi}$ but only the most negative value is stable: the wafer can be inverted by heating (or mechanically) but can only be restored if heated by reversing the direction of thermal gradients. This response is verified in Fig. 2 for $\bar{\kappa}_0$ equal to $2.5/\sqrt{\phi}$. Opposite-sense heating produces a very pronounced S-curve, which intersects the vertical axis at three distinct points when $\bar{\kappa}_T = 0$, and the stable portions of the curve are synonymous with positive local gradients. In practice, heating cannot be increased beyond $\bar{\kappa}_T = -34$ without a sudden jump, or *snap-through,* in displacements from approximately $-3t$ to $-12.5t$, in order to follow the equilibrium path. Cooling the wafer follows the curve back to, and past, the stable inverted position to $\bar{\kappa}_T = 10$ before

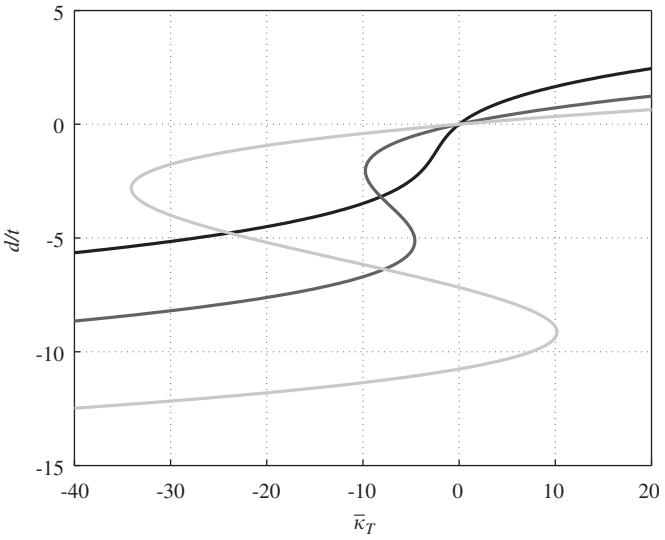

Fig. 2. Predictions of axi-symmetrical displacements of three spherical wafers via Eq. (21) in which $\bar{\kappa}_0 = 0.5/\sqrt{\phi}$ (black), $\bar{\kappa}_0 = 1.5/\sqrt{\phi}$ (dark grey) and $\bar{\kappa}_0 = 2.5/\sqrt{\phi}$ (light grey), with $\phi = (1-\nu)/16$. The wafer properties are standard, as in Table 1.

jumping back to the positive part of the curve. Two other curves are also detailed for completeness: for $\bar{\kappa}_0 = 0.5/\sqrt{\phi}$, there are no inflexion points, and for $\bar{\kappa}_0 = 1.5\sqrt{\phi}$, the gentle S-curve has only one root at the origin.

The curvatures, $\bar{\kappa}_x$ and $\bar{\kappa}_y$, are linearly related in the second mode, but they must also satisfy Eq. (15b) in which the change in Gaussian curvature, now designated as $\bar{\kappa}_x\bar{\kappa}_y - \bar{\kappa}_0^2$ for no twisting, is a constant. This mode is developable, as for a flat wafer, and the ultimate solutions for $\bar{\kappa}_x$ and $\bar{\kappa}_y$ are found to be

$$\bar{\kappa}_x = \frac{(1+\nu)}{2}[\bar{\kappa}_T + \bar{\kappa}_0]\left(1 + \left[1 - \left(\frac{\bar{\kappa}_0 + \bar{\kappa}_T^*}{\bar{\kappa}_0 + \bar{\kappa}_T}\right)^2\right]^{0.5}\right),$$

$$\bar{\kappa}_y = \frac{(1+\nu)}{2}[\bar{\kappa}_T + \bar{\kappa}_0]\left(1 - \left[1 - \left(\frac{\bar{\kappa}_0 + \bar{\kappa}_T^*}{\bar{\kappa}_0 + \bar{\kappa}_T}\right)^2\right]^{0.5}\right), \tag{22}$$

where $\bar{\kappa}_T^*$ is the heating at the bifurcation between cases, obtained by inspecting the relative degrees of stored energy as

$$\bar{\kappa}_T^* = -\bar{\kappa}_0 + \frac{2}{1+\nu}\left[\frac{16}{1+\nu} + \bar{\kappa}_0^2\right]^{0.5}$$

and the corresponding wafer curvature is

$$\bar{\kappa}^* = \left[\frac{16}{1+\nu} + \bar{\kappa}_0^2\right]^{0.5}.$$

A comparison between this approximate solution and a finite element analysis is presented in Fig. 3. For positive heating in which $\bar{\kappa}_T$ produces curvature changes in the same sense as $\bar{\kappa}_0$, the behaviour is similar to Fig. 1 but with lower predictions of both values of $\bar{\kappa}_T^*$ compared to the simulation. Opposite-sense heating is recovered by assigning a negative value to $\bar{\kappa}_0$, all other parameters being

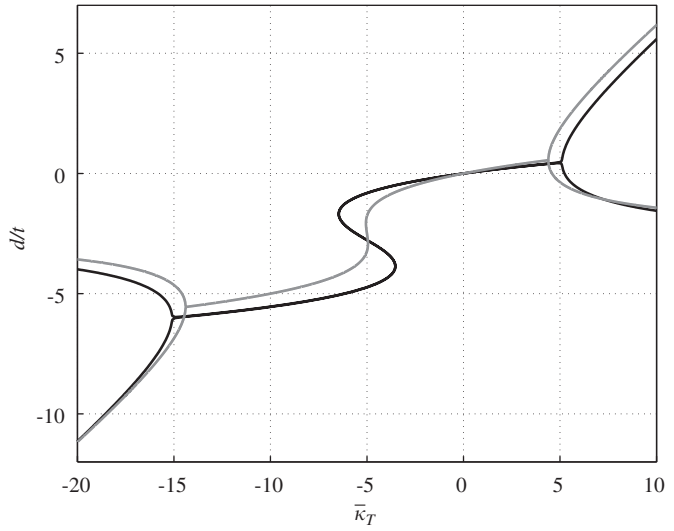

Fig. 3. Predictions of maximum and minimum out-of-plane displacements compared to finite element analysis of a spherical wafer with $\bar{\kappa}_{x0} = \bar{\kappa}_{y0} = 5$. The wafer properties are standard, as in Table 1. The grey lines are theoretical predictions for axi-symmetrical behaviour, Eq. (21), and for diverging behaviour ($\bar{\kappa}_T > 5$ or $\bar{\kappa}_T < -15$), Eq. (22). Finite element results are shown as black lines.

positive; but for plotting purposes, the signs are reversed. The simulation has the same S-curve associated with snap-through behaviour, but there are no stable inverted positions, for this example.

The axi-symmetrical prediction underestimates the rate of change of stiffness and severity of the snap-through behaviour in the region of $\bar{\kappa}_T = -5$. The data is masked by the range of heating but there is a slight S-curve since the selected magnitude of $\bar{\kappa}_0$, equal to 5, is just greater than the critical value, $1/\sqrt{\phi} = 0.478$ for $\nu = 0.3$. The most likely reason for the discrepancy is that the wafer curvature is not uniform. A quick confirmation is provided in Fig. 4 where the wafer shape at the first stationary point, $(\bar{\kappa}_T, d/t) \approx (-6.25, -2)$, can be compared to a circular arc, drawn to have the same curvature as points near the edge, but not necessarily elsewhere. Clearly, the arc does not fit the wafer profile in the centre, and the curvature is not the same throughout. Further evidence can be gleaned from the early work of Wittrick et al. [8] on bimetallic domes. They considered higher-order terms in the displacement profile, but pursue a numerical solution to yield a lower bound value of $\bar{\kappa}_0$ of about $8.9/\sqrt{6(1-\nu^2)} \approx 3.8$ for $\nu = 0.3$, for snap-through to prevail; for a value of 5 here, the S-curve ought to be well developed, as demonstrated by the computational results. Nonetheless, the axi-symmetrical prediction outside the region of snap-through generally agrees very well, and the bifurcations do not feature in Wittrick's study.

3.3. Cylindrical wafer

For the singly curved case, $\bar{\kappa}_{x0} = \bar{\kappa}_0$ and $\bar{\kappa}_{y0} = 0$, Eq. (13) does not have linear factors, and there is a single,

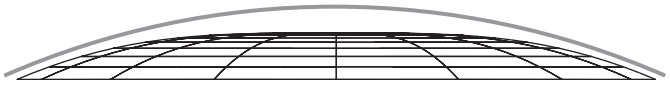

Fig. 4. Side-view of the wafer from Fig. 3 at the first stationary point on reverse heating, $\bar{\kappa}_T \approx -6.25$ and $d/t \approx -2$. The displacements have been amplified tenfold for clarity, and the outline profile indicates the wafer curvature along a given meridian. The grey circular arc, of constant curvature, is drawn as a best fit to points only near the edge. The wafer is much less curved in the centre where the departure of the arc from its surface reaches a maximum distance.

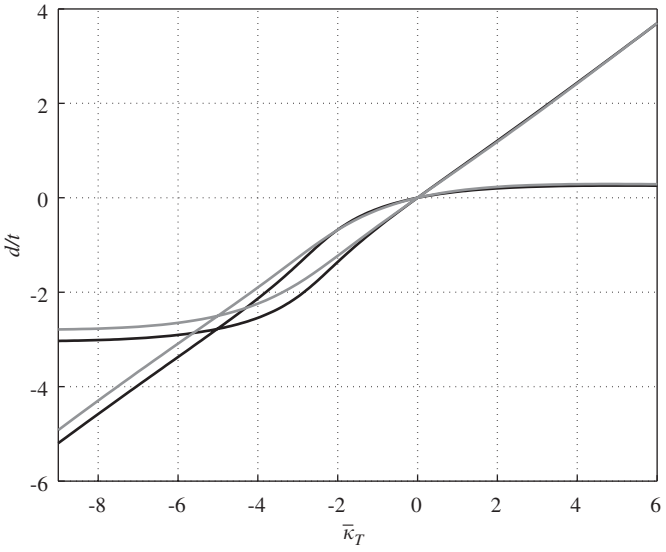

Fig. 5. Predictions of maximum and minimum out-of-plane displacements compared to finite element analysis of a cylindrical wafer with $\bar{\kappa}_{x0} = 5$ and $\bar{\kappa}_{y0} = 0$. For positive heating, the linear displacement derives from $\bar{\kappa}_x$, whilst for reverse heating, the same curvature produces a non-linear displacement, and vice versa. Numerical solutions of the equations of the approximate theory, Eq. (12), are shown as grey lines; black lines are obtained from a finite element analysis and, for $\bar{\kappa}_T > 0$, are overlapped by the close numerical predictions.

non-developable mode of deformation and no direct closed-form solutions for $\bar{\kappa}_x$ and $\bar{\kappa}_y$. The simplest route, however, solves numerically for them by, for example, admitting Eqs. (12a)–(12c) to a least-squares solution approach using the software package, MATLAB [15]. In this way, $\bar{\kappa}_{xy}$ is always returned as zero, and computation of the corresponding eigenvalues of the generalised stiffness matrix in Eq. (20) confirm modal stability.

A typical set of results is given in Fig. 5, along with a finite element analysis. For positive heating, the numerical and computational solutions are practically the same, and show that the displacements under $\bar{\kappa}_x$ and $\bar{\kappa}_y$ diverge straightaway, with increased cylindrical distortion in the x direction. Initially straight generators along the y-axis are perturbed slightly into a gentle arc but appear to reach a shallow limiting value. Asymptotic solutions to Eq. (13) are therefore suggested as $\bar{\kappa}_y = 0$ and $\bar{\kappa}_x = \bar{\kappa}_0 + (1+\nu)\bar{\kappa}_T$, and are confirmed at much higher values of $\bar{\kappa}_T$, but not recorded here. Physically, the wafer accrues some

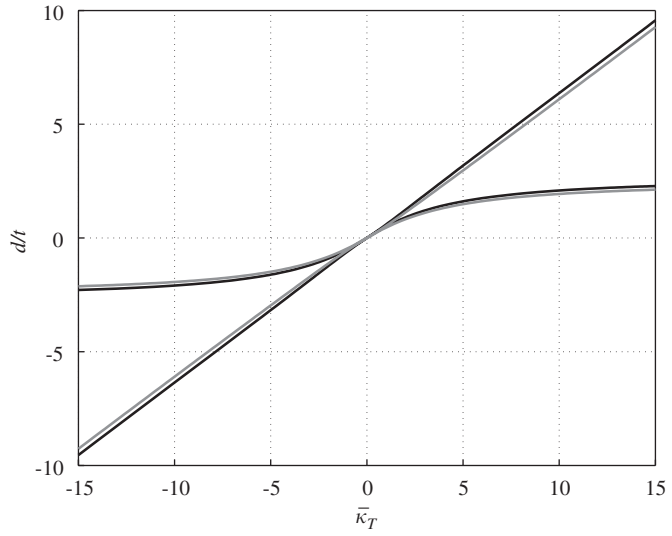

Fig. 6. Predictions of maximum and minimum out-of-plane displacements compared to finite element analysis of a saddle-shaped wafer with $\bar{\kappa}_{x0} = 5$ and -5. For $\bar{\kappa}_T > 0$, the larger displacements pertain to $\bar{\kappa}_x$ and vice versa. Black lines belong to a finite element analysis and grey lines are numerical predictions.

Gaussian curvature from zero but it is already pre-disposed to a cylindrical mode, and cannot switch into another developable mode, as in the flat or spherical cases. There is a small but diminishing change in the Gaussian curvature as heating progresses.

For reverse heating, the cylindrical deformation now favours the flat y direction over the oppositely curved x-axis, which must unbend first before curving in the same sense. Around $\bar{\kappa}_T = -5$, the displacements are the same and the curvatures are anti-symmetrical and inverted, $\bar{\kappa}_y \approx -\bar{\kappa}_0$ and $\bar{\kappa}_x = 0$, compared to the start; thereafter, the asymptotic form is repeated but the development of principal curvatures has swapped. Predictions of behaviour are fairly good for larger values of $\bar{\kappa}_T$.

3.4. Saddle wafer

Finally, consider a wafer with $\bar{\kappa}_{x0} = -\bar{\kappa}_{y0} = \bar{\kappa}_0$, resulting in a saddle shape, which may be viewed as being purely twisted with respect to the axes defined by the lines $y = x$ and $-x$. Despite the exact anti-symmetry Eq. (13) does not factorise, but a set of stable solutions may be extracted in the same numerical manner as before, see Fig. 6.

The correlation with the finite element analysis is exceptionally close and, as might be expected, the response is anti-symmetrical about the origin. For either direction of heating, the wafer continues to bend cylindrically about the axis of positive curvature whilst relieving most of the other principal curvature. The asymptotic solutions, e.g. for positive heating, $\bar{\kappa}_x = \bar{\kappa}_0 + (1+\nu)\bar{\kappa}_T$ and $\bar{\kappa}_y = 0$, indicate a limiting change of $\bar{\kappa}_y = 0$ in the Gaussian curvature as the wafer tends towards a developable surface.

4. Summary

This study has been concerned with the elastic response of a thin wafer with through-thickness thermal gradients. The motivation has been to gain an understanding of semi-conductor treatment processes, such as the flashlamp irradiation of heteroepitaxial layers of SiC on silicon, which depend on the imposition of non-linear temperature distributions, thereby risking excessive deflexions and mechanical failure of the wafer. Here, the quasi-statical heated response has been established for a circular, constant thickness wafer with general initial distortions from the flat. The displacement fields are derived from the assumption of uniform changes in curvature of the wafer, which violates the moment-free boundary condition at the edge; but it enables a relatively straightforward strain energy formulation, in which powerful concepts associated with the Gaussian curvature performance of the wafer provide an elegant, compact description of the bending–stretching interaction. The robustness of the predictions has been confirmed through some very good correlations with a more sophisticated finite element analysis, which lacks the assumption of uniform curvature, for a number of different wafer geometries. Conditions for bifurcation and snap-through buckling phenomena have been distilled. Finally, all results may be extended to generally distorted wafers with locked-in stresses of the type studied by Freund [6] by simply interchanging some terms as described in the Appendix.

Acknowledgments

We are grateful to our colleague, C.R. Calladine, Professor Emeritus, for his valuable input to this study. A reviewer is thanked for insightful comments.

Appendix

This study obtains the same dimensionless bifurcation curvature as Freund [6] who considers the uniform curving of a flat, composite wafer substrate and thin film under locked-in stresses, as if the film was removed, tensioned and re-attached to the substrate. The inherent mismatch in Freund's wafer depends on the degree of interfacial strain, ε_m, and in dimensionless form is implied within his expression

$$S = \frac{3\varepsilon_m a^2 h_f M_f}{2h_s^3 M_s}, \tag{23}$$

where subscripts f and s refer to the film and substrate, each of thickness h_f and h_s, and elastic modulus, M_f and M_s. The critical value, S^*, to cause buckling into an asymmetrical mode is found by Freund to be $2/(1+\nu)^{3/2}$. In a very early study, Stoney [16] separately establishes the freely developed substrate curvature, K_{st}, as

$$\kappa_{st} = \frac{6f}{h_s^3 M_s} \tag{24}$$

in which f is the membrane force per unit length on the middle surface of the composite wafer; this quantity is equal to $M_f\varepsilon_m h_f$ and, if it is substituted back into κ_{st}, which is then made dimensionless by multiplying by a^2/t where t is total thickness, it can be shown that

$$\bar{\kappa}_{st} = 4S \Rightarrow \bar{\kappa}^*_{st} = 4S^* = \frac{8}{(1+\nu)^{3/2}} \tag{25}$$

and is identical to $\bar{\kappa}^*_T$ in Eq. (18). The result is obvious from the simple fact that both the effects of heating and mismatch are represented by the integral curvature parameters, κ_T and κ_{st}; and the responsible physical mechanisms are not apparent in the mathematical formulation.

References

[1] Panknin D, Stoemenos J, Eickhoff M, Heera V, Vouroutzis N, Krotz G, et al. Improvement of the 3C-SiC/Si interface by flashlamp annealing. Materials Science Forum 2000;353–356:151–4.

[2] Smith MP, McMahon RA, Voelshow M, Skorupa W. Modelling and regrowth mechanisms of flashlamp processing of SiC-on-silicon heterostructures. Journal of Applied Physics 2004;96(9):4843–51.

[3] Mansfield EH. The Bending & Stretching of Plates. Cambridge: Cambridge University Press; 1989.

[4] Mansfield EH. On the analysis of elastic plates of variable thickness. Quarterly Journal of Mechanics and Applied Mathematics 1962;15:167–92.

[5] Mansfield EH. Bending, buckling and curling of a heated thin plate. Proceedings of the Royal Society, London A 1962;268(1334): 316–27.

[6] Freund LB. Substrate curvature due to thin film mismatch strain in the nonlinear deformation range. Journal of the Mechanics and Physics of Solids 2000;48:1159–74.

[7] Timoshenko S, Woinowsky-Krieger S. Theory of Plates and Shells. Engineering Societies Monographs, second ed. New York: McGraw Hill; 1959.

[8] Wittrick WH, Myers DM, Blunden WR. Stability of a bimetallic disk. Quarterly Journal of Mechanics and Applied Mathematics 1953;6(1):15–31 [Parts I and II].

[9] Dano ML, Hyer MW. Snap-through of unsymmetric fiber-reinforced composite laminates. International Journal of Solids and Structures 2002;39:175–98.

[10] Calladine CR. Theory of Shell Structures. Cambridge: Cambridge University Press; 1983.

[11] Guest SD, Pellegrino S. Analytical models for bistable cylindrical shells. Proceedings of the Royal Society, London A 2006;462: 839–54.

[12] Hibbitt, Karlsson, and Sorenson. ABAQUS Version 5.8. Pawtucket: Hibbitt, Karlsson & Sorenson, Inc.; 1998.

[13] Riks E. The application of Newton's method to the problem of elastic stability. Journal of Applied Mechanics 1972;39:1060–6.

[14] Seffen K.A. Heating of a thin uniform disk by finite elements. Technical Report CUED/D-STRUCT/TR 217. Cambridge University; 2005.

[15] MathWorks. Matlab R12. Natick, MA 01760-2098, USA, 2000.

[16] Stoney GG. The tension of metallic films deposited by electrolysis. Proceedings of the Royal Society, London A 1909;82:172–5.